International Journal of Thermal Sciences 124 (2018) 484–495

Contents lists available at ScienceDirect

International Journal of Thermal Sciences

journal homepage: www.elsevier.com/locate/ijts

Effect of channel inclination on heat transfer and bubble dynamics during subcooled flow boiling

Maria C. Vlachou, Thodoris D. Karapantsios*

Faculty of Chemistry, Division of Chemical Technology, Aristotle University of Thessaloniki, University Box 116, 54124, Thessaloniki, Greece

ARTICLE INFO

Keywords:
Heat transfer coefficient
Inclined channel
Flow orientation
Bubble diameter
Bubble density
Bubble velocity

ABSTRACT

This study explores the influence of inclination on highly subcooled flow boiling of water in a macro-channel 10 mm high, 40 mm wide and 120 mm long. Experiments have been conducted under the following conditions. Channel inclination: 0°, 30°, 45°, 60°, 90°, 120°, 150°; mass flux: 330, 630, 830 kg/m^{2}s; heat flux in the range 300–1000 kW/m^2. Temperature recordings allow analysis of channel's heat transfer performance, while high speed video recordings provide evidence of bubbles' features. A comparative thermal and optical examination is presented for the transition region (low-heat-flux), and the nucleate boiling region (high-heat-flux). In the examined range of parameters, boiling curves are influenced more by mass flux than by inclination. Overall, operation at 60° and 90° yields higher heat fluxes than at other inclinations but the effect never exceeds an increase of 10% in the heat transfer coefficient compared to the horizontal case. Experimental heat transfer coefficients are in reasonable accordance with predictions of well-known empirical correlations. The role of inclination on heat transfer is explored via the analysis of bubbles' size, area density and sliding velocity. The observed bubble dynamics are in line with the measured boiling curves and heat transfer coefficients.

1. Introduction

Flow boiling is a preferable cooling method in a plethora of applications because of the associated high heat transfer rates. In flow boiling, two complex phenomena are involved, forced convection of bulk liquid and growth/detachment of bubbles at the heated surface [1]. Understanding these phenomena is essential for increasing the efficiency and for optimizing the operation of two-phase heat exchange devices. In particular, the important role of bubbles in two-phase heat transfer mechanisms necessitates the study of bubbles behavior and their interaction in analyzing the thermal performance of heat exchangers [2].

In the absence of forced flow, pool boiling investigations have shown that changing the inclination of a heated surface from horizontal facing upwards (θ = 0°) to horizontal facing downwards (θ = 180°), leads to different boiling regimes, owing to different force balance between surface tension, buoyancy and bubble growth inertia [3]. Heat transfer coefficient, h increases when bubbles grow isolated and detach promptly from the surface and when sliding occurs (on inclined surfaces) whereas it decreases when bubbles accumulate and coalesce to form gas films covering the surface [4–6]. The presence of flow, apart from the additional forced convection term in the energy balance, imparts one more term in the bubble force balance, the hydrodynamic force, influencing boiling regimes [7]. Depending on the size of the boiling channel/tube (micro-, mini-, macro-) boiling regimes differentiate [8]. In micro-channels, due to the restricted size and vapor confinement, slug, churn and annular are the most common regimes, with no distinctive bubble dynamic behavior [9]. In mini- and macro-channels, however, dispersed bubbly flow often prevails either parallel to the heated surface after some (short or long) sliding or normal to the heated surface without sliding (lift-off) [10].

Inclination of the flow with respect to the horizontal plane (θ = 0°) can enhance boiling heat transfer rates by facilitating bubbles removal from the heated wall and liquid replenishment over the wall [7]. It has been reported that in macro- and mini-channels the effect of inclination on flow boiling is felt mostly at liquid velocities below 1 m/s [11,12], which are associated with weak inertia [13]. Investigation of channel inclination, θ, during flow boiling has attracted much attention over the past years for two reasons. One is the influence that it can have on bubbles interfacial behavior and on heat transfer performance [11], and the other is that it constitutes a fast and easy way to simulate effects encountered in experiments at modified, e.g., reduced, gravity conditions, since each θ produces different partial components of gravity normal and parallel to the heated wall [10,13]. On this common ground, several researchers conducted flow boiling experiments to examine the effect of θ on heat transfer or on bubble dynamics in tubes

* Corresponding author.
E-mail address: karapant@chem.auth.gr (T.D. Karapantsios).

https://doi.org/10.1016/j.ijthermalsci.2017.10.041
Received 31 January 2017; Received in revised form 24 October 2017; Accepted 24 October 2017

Nomenclature

A	heat exchange area, m^2
A_p	parameter defined by equation (11)
Bo	Boiling number ($q'' G^{-1} \Delta H^{-1}$)
C	parameter defined by equation (13)
C_p	specific heat, J $kg^{-1} K^{-1}$
D_h	hydraulic diameter, m
D_{HP}	heated equivalent diameter, m
D	bubbble diameter, m
F	darcy friction factor, -
g	gravitational constant, m s^{-2}
G	mass flux, kg $m^{-2} s^{-1}$
h	heat transfer coefficient, W $m^{-2} K^{-1}$
Ja	Jacob number ($\rho_l C_{pl} \Delta T_{wall} \rho_v^{-1} \Delta H^{-1}$)
k	thermal conductivity, W $m^{-1} K^{-1}$
L	channel length, m
l_e	entrance length, m
M	molecular weight, kg mol^{-1}
N/A	bubble density, m^{-2}
P	pressure, bar
p_r	reduced pressure, - (absolute pressure/critical pressure)
Pr	Prandl number ($C_p \mu k^{-1}$), -
Q	volumetric flow rate, $m^3 s^{-1}$
q*	parameter defined by equation (12)
q″	heat flux, W m^{-2}
Re	Reynolds number ($\rho u D_h \mu^{-1}$), -
S	parameter defined by equation (14)
T	temperature, °C
V_b	volume of a bubble, m^3
u	velocity, m s^{-1}
w	channel width, m
x	channel height, m

Greek symbols

ΔH	latent heat of vaporization, J kg^{-1}
ΔT	temperature difference, °C
Δx	distance, m
μ	dynamic viscosity, N s m^{-2}
ρ	density, kg m^{-3}
σ	surface tension, N m^{-1}
θ	inclination angle, °

Subscripts

aver	average
exp	experimental
f	film
FC	forced convection
in	inlet
l	liquid
mid	middle
mix	mixing cup
OBR	Onset of Bubbly Regime
ONB	Onset of Nucleate Boiling
Out	outlet
sat	saturation
sub	subcooling
v	vapor
theor	theoretical
wall	heatd wall

and channels, with only limited information provided about both effects simultaneously. First, works about refrigerants flow boiling in mini- and macro-channels/tubes are presented, being followed by water flow boiling investigations.

Flow boiling experiments with refrigerants R-134a and R407C in macro-tubes have been reported by Akhavan-Behabadi and Esmailpour [14] (D: 8.3 mm) and Kundu et al. [15] (D: 7 mm), respectively. Both studies reported the highest heat transfer coefficient, h, at 90° (vertical upward flow), and noted that θ effect is stronger at low vapor qualities (< 0.5). However, they did not investigate bubbles behavior. Zhang et al. [11,16] employed photographic evidence to identify different critical heat flux, CHF, regimes during saturated and subcooled flow boiling of FC-72 in a macro-channel (×5 mm, w2.5 mm, L101.6 mm) at different inclinations. According to their results, CHF reached a maximum value at 45°, where buoyancy helped the most to detach vapor bubbles from the heated surface, and dropped to a minimum at 225°, where vapor was mostly accumulating on the heated surface. Konishi et al. [17] and Kharangate et al. [13,18] performed flow boiling experiments in the same geometry as Zhang et al. featuring one or two opposite facing heated walls at different θ with focus on gravity effects on interfacial behavior. A peak in h was noticed at 90°, where both single-sided and double-sided heating showed better symmetry in vapor formation along the channel compared to other inclinations. Although the above works argue about effects of θ on interfacial behavior, they only report overall heat transfer results (h or CHF) and overall visual observations about the identified boiling regimes, without any information on bubble dynamics (bubble sizes and velocities).

Sugrue et al. [19] carried out flow boiling experiments with water in a rectangular mini-channel (×1.99 mm, w1.43 mm, L317.5 mm) focusing on results of departure diameters of sliding bubbles at a single value of heat flux (100 kW/m^2). They found that bubble departure diameter reached a minimum at 90°, because the tangential component of the buoyancy force is largest at that angle, but differences at various θ were very small (about 15% between 0° and 90°). There are few more studies where bubbles monitoring and bubble dynamics analysis in water flow boiling have been conducted at 90°, at various channel sizes (D_h: 3.8–19.1 mm) and different subcoolings (ΔT_{sub}: 2–75 °C) [12,20–25]. However these studies are limited to the vertical orientation and a single value of heat flux for most of the cases while they do not attempt a comparison with other inclinations or a correlation of bubbles behavior with heat transfer results.

To our knowledge this is the first study combining systematically thermal and optical results at different inclinations (θ: 0-150°) in a macro-channel (×10 mm, w40 mm, L120 mm). The current study examines the effect of θ on heat transfer characteristics (onset of nucleate boiling, onset of bubbly regime, boiling curve, heat transfer coefficient, heat transfer mechanism) and on bubble dynamics (bubble size distribution, bubble density, bubble sliding velocity) under various mass fluxes (G: 330–830 kg/m^2s) and heat fluxes (q″: 300–1000 kW/m^2). The working fluid is water, a choice chiefly motivated by the need to investigate fast cooling of hot hollow walls by internal water flow at extreme conditions (i.e. fire incidents in space vehicles) [26]. For the same reason, a high inlet subcooling (ΔT_{sub} = 70 °C) is employed as this increases CHF [13,17] by hindering dryout [18,23]. Comparison of results among different inclinations as well as with observations by other researchers offers a thorough insight of bubble's contribution to heat transfer under various gravity effective components.

2. Materials and methods

2.1. Experimental device and procedure

The experimental setup is schematically presented in Fig. 1a and consists of the test section adjusted at a flow loop. A detailed

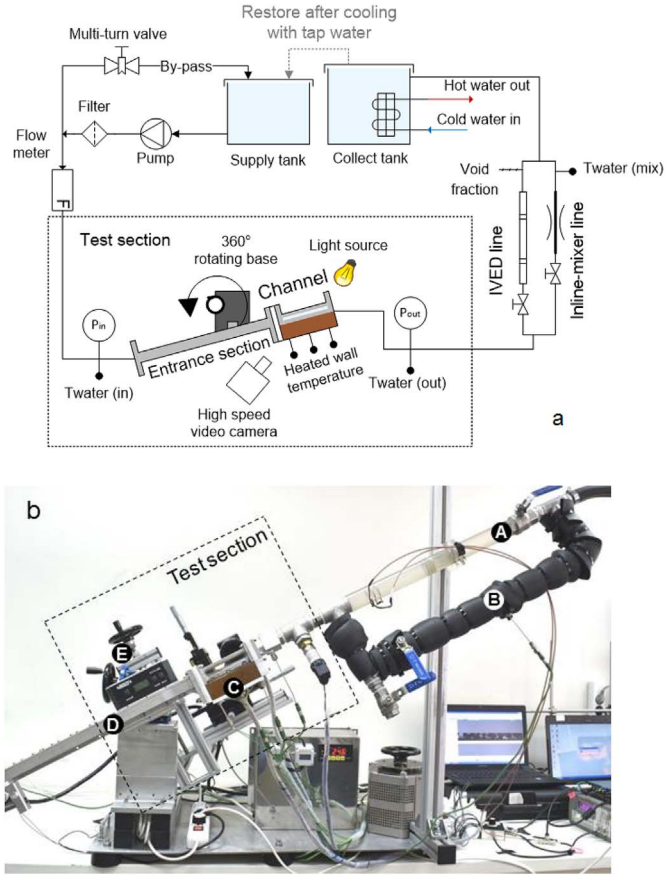

Fig. 1. Illustrations of the experimental device (a) schematic graph, (b) photograph.

description of the experimental setup and diagnostics is given in Vlachou et al. [27]. A brief description is made here. The working fluid is deionized water. Large amount of water (500 L) is stored in a supply tank to allow achieving steady state conditions at the employed high flow rates. Water is circulated by a progressive cavity pump (Sydex, K-032-1S, 1 hp) that prevents cavitation. Fig. 1b displays the test section without insulation for demonstration purposes. Outlet is divided in two parallel lines, which are operated individually; a line for void fraction measurement (A) made of polycarbonate transparent tube (IVED-line) and a line for mixing-cup temperature measurement (B) equipped with an in-line static mixer (Inline-mixer line). IVED is an ultra-sensitive impedance technique [28] capable of recording the void fraction of two-phase streams. In this study, however, no void fraction measurements are conducted because of the high degree of subcooling, which makes most bubbles re-condense before reaching the measurement point.

The test section is composed of the heated channel (C) of orthogonal cross-section (×10 mm, w40 mm, L120 mm) and the unheated entrance section (D) of the same cross-section having sufficient length to achieve fully developed flow (l_e = 500 mm). The particular channel dimensions are chosen to resemble those of a low gravity experiment onboard the International Space Station, RUBI [29]. The entrance section is stably attached to a 360° rotating base (E), which allows the test section attaining any inclination around a full circle. The channel (Fig. 2) consists of a copper block (heater) coupled with an aluminum frame of Π shape. The top surface of the copper block (40 × 120 mm) acts as the boiling surface; the channel is heated only from one side. The aluminum frame has transparent ceramic windows (Schott Robax®) from all three sides to allow optical observations. Electrical heating is achieved by 14 cartridge heaters accommodated in the copper block capable of delivering maximum power of 5.5 kW.

Volumetric flow rate is measured by a paddle wheel transmitter (Burkert 8035, range 0.3–10 m/s, accuracy ± 2.5% of measured value). Pressure is recorded at the inlet, prior to the entrance section, and at the outlet of the heated channel, with two absolute pressure transducers (Wika S-10, range 0–2.5 bar, accuracy < 0.25% of span). Inclination is measured by a digital level meter and protractor (InSize 2173-360, accuracy ± 0.2°). A high speed video camera (Mikrotron, Motionblitz, Eosens mini 2, 60 mm macro lens) is employed to record bubble dynamics from the side window of the channel, 10 mm before the channel's outlet, capturing images between 8000 and 10000 fps. The images resolution is 5 μm/pixel. Working fluid and heated wall temperatures are obtained by K-type, ungrounded thermocouples (Uteco, 2 mm, accuracy after calibration ± 0.1 °C). The temperature of the working fluid is acquired at the inlet (T_{in}) of the entrance section, at the outlet of the channel (T_{out}) and right after the location of the inline-mixer (T_{mix}). The temperature inside the copper block is measured at 6 positions (Fig. 2) by pairs of thermocouples; 10 mm after the inlet and 10 mm before the outlet of the channel (2 mm below the boiling surface), as well as in the middle of the channel (one 2 mm and one 12 mm below the boiling surface).

All experiments are conducted at atmospheric pressure. At steady state, continuous recordings of flow rate, temperature and pressure are made for a period of 1 min and high speed video recordings for intermittent periods of 1s. At every set of experimental conditions at least three runs are conducted to check for repeatability and allow estimation of statistical quantities. Error bars are added to all data markers in the plots representing their standard deviation. Table 1 summarizes the employed working conditions.

Supplementary video related to this article can be found at http://dx.doi.org/10.1016/j.ijthermalsci.2017.10.041.

2.2. Data reduction

The following parameters are calculated:

Average bulk liquid temperature (T_{aver})

$$T_{aver} = \frac{T_{in} + T_{mix}}{2} \quad (1)$$

Film temperature between the liquid and the heated wall temperature (T_f)

$$T_f = \frac{T_{wall} + T_{aver}}{2} \quad (2)$$

Temperature differences of subcooling (ΔT_{sub}) and wall superheat (ΔT_{wall})

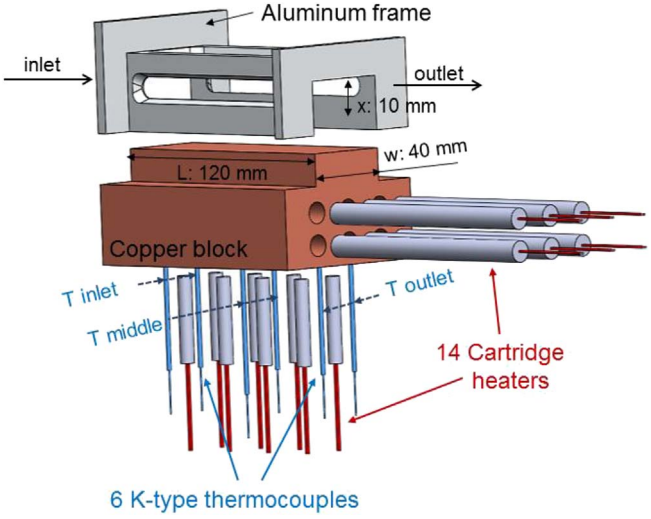

Fig. 2. Schematic diagram of the channel configuration.

Table 1
Working conditions.

Parameter	Value/Range	Unit
Subcooling inlet, ΔT_{sub}	70	°C
Subcooling outlet, ΔT_{sub}	62.7–69.5	°C
Mass fluxes, G	330, 630, 830	kg/m^{2}s
Liquid velocity, u_l	0.33, 0.63, 0.83	m/s
Heat fluxes, q″	200–1000	kW/m^2
Channel dimensions	×10, w40, L120	mm
Inclinations	0, 30, 45, 60, 90, 120, 150	°

$$\Delta T_{sub} = T_{sat} - T_{in} \tag{3}$$

$$\Delta T_{wall} = T_{wall} - T_{sat} \tag{4}$$

T_{sat} is the saturation temperature at the pressure of the fluid. T_{wall} is the average wall temperature calculated by applying Fourier law of conduction inside the copper block using as inputs the temperatures measured 2 mm below the heated surface.

The heat flux provided to the liquid (q″) is calculated by Fourier law using as inputs the measured temperature difference of the two middle thermocouples that are positioned 10 mm apart from each other in the direction of heat flow.

$$q'' = -k\,\frac{\Delta T_{mid}}{\Delta x_{mid}} \tag{5}$$

k is copper's thermal conductivity.

The average flow boiling heat transfer coefficient (h)

$$h = \frac{q''}{T_{wall} - T_{aver}} \tag{6}$$

2.3. The mass flux (G)

$$G = \frac{Q\cdot\rho_{in}}{x\cdot w} \tag{7}$$

Reference values for the heat transfer coefficient are calculated for comparison with those experimentally obtained. In the forced convection region (single phase), h_{FC} is estimated from the correlation of Gnielinski [30], with the friction factor, f, obtained from Moody's diagram for a smooth pipe, the hydraulic diameter D_h for rectangular channel defined as $D_h = \frac{2xw}{x+w}$ and with the fluid properties calculated at the film temperature, T_f.

$$h_{FC} = \frac{Nu\cdot k}{D_h} \tag{8}$$

$$Nu = \frac{\frac{f}{8}(Re - 1000)\cdot Pr}{1 + 12.7\left(\frac{f}{8}\right)^{\frac{1}{2}}\left(Pr^{\frac{2}{3}} - 1\right)} \tag{9}$$

Gnielinski predictions are reported to describe experimental values usually within ± 15%. Reference values for the heat transfer coefficient in the subcooled flow boiling region, h, are estimated from empirical correlations for mini- and macro-channels and tubes [31,32]. For the correlation developed by Liu and Winterton [31] p_r is the reduced pressure, M the molecular weight and fluid properties are calculated at T_{aver}.

$$h = \frac{\sqrt{(A_P\, S\, \Delta T_{wall})^2 q''^{\frac{4}{3}} - q''^2}}{\Delta T_{wall}}\cdot q_*^{\frac{3}{2}} \tag{10}$$

$$A_P = 55\cdot p_r^{0.12}\,(-\log p_r)^{-0.55}\, M^{-0.5} \tag{11}$$

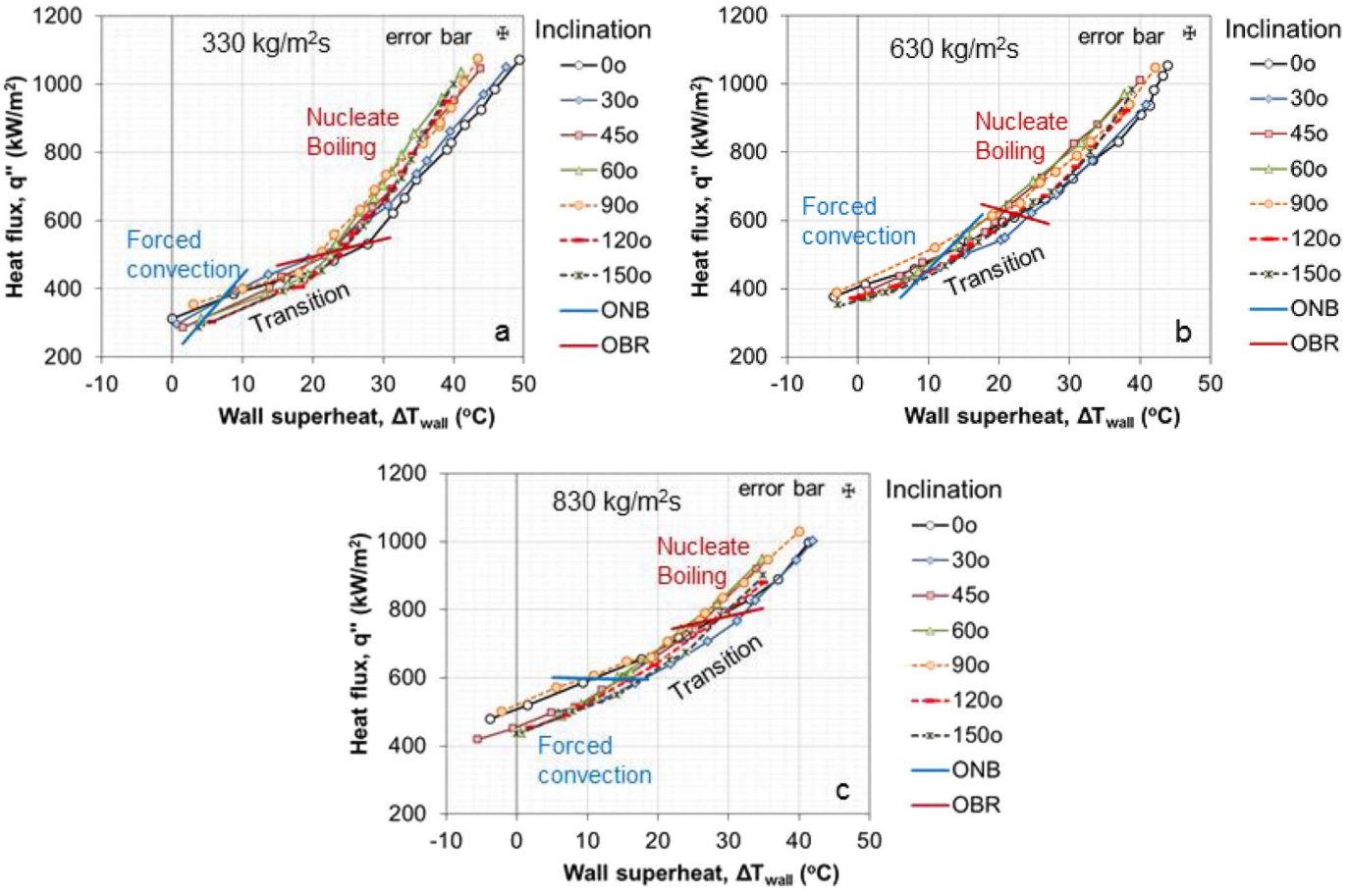

Fig. 3. Effect of channel inclination angle on boiling curves for different mass fluxes (a) 330 kg/m^{2}s, (b) 630 kg/m^{2}s and (c) 830 kg/m^{2}s.

$$q_*^3 - C\,q_*^2 - 1 = 0 \tag{12}$$

$$C = \left(\frac{A_P\,S}{h_{FC}}\right)^2 \left[\frac{\sqrt{(A_P\,S\,\Delta T_{wall})^2 q^{\frac{4}{3}} - q^2}}{\Delta T_{wall}} \cdot (T_{wall} - T_{aver})\right]^{\frac{4}{3}} \tag{13}$$

$$S = (1 + 0.055\,Re^{0.16})^{-1} \tag{14}$$

Liu and Winterton predictions are reported to describe experimental values within ± 40%.

For the correlation developed by Shah [32] h_{FC} is calculated by Dittus and Boelter [33] and fluid properties at T_{aver}.

$$h = \frac{h_{FC}(T_{wall} - T_{aver}) + h_{FC}(\psi_0 - 1)\Delta T_{wall}}{T_{wall} - T_{aver}} \tag{15}$$

$$\text{Larger value between } \psi_0 = 230Bo^{0.5} \text{ and } \psi_0 = 1 + 46Bo^{0.5} \tag{16}$$

$$h_{FC} = 0.023Re^{0.8}\frac{Pr^{0.4}k}{D_h} \tag{17}$$

Shah predictions are reported to describe experimental values within ± 30%.

Mean absolute percentage error (MAPE) between the experimental (h_{exp}) and the predicted value (h_{theor}) of h is given by:

$$MAPE = \left[\frac{1}{N}\sum_1^N ABS\left(\frac{h_{theor} - h_{exp}}{h_{exp}}\right)\right]\cdot 100 \tag{18}$$

Bubble diameter (d) and bubble density (Number of bubbles/Area, N/A) are measured manually in a series of frames at each run. At least 1000 individual bubbles per run are accounted in these calculations. Bubble velocity (u) is obtained from bubble's traveling distance between frames of known time interval. At least 10 individual bubbles per bubble size are accounted in these calculations.

3. Results and discussion

3.1. Effect of inclination on heat transfer characteristics

3.1.1. Boiling curve

Plotting heat flux, q″, versus wall superheat, ΔT_{wall}, for different set of conditions yields boiling curves with regards the employed mass flux, G, and inclination, θ. Fig. 3 shows the effect of inclination on boiling curves for three mass fluxes, namely, 330, 630 and 830 kg/m^{2}s. All curves exhibit trends observed in a typical boiling curve; those are (a) the single-phase forced convection region at low ΔT_{wall} at which no bubbles appear (purely liquid flow), (b) the nucleate boiling region at high ΔT_{wall} where boiling is intense and many bubbles are present, (in literature is also called fully developed nucleate boiling region) and (c) the transition region between the forced convection and nucleate boiling regions. This intermediate region can be also found in literature termed as local boiling, partial boiling or highly subcooled boiling. Onset of nucleate boiling (ONB; blue line in Fig. 3) is designated by the first bubble's appearance on the boiling surface as detected by high speed images. On the other hand, onset of bubbly regime (OBR; red line in Fig. 3), is identified by the abrupt rise in the slope of the boiling curve which demarcates nucleate boiling domination over forced convection [27]. It is apparent that θ has only a small influence on boiling curves with inclinations of 60° and 90° performing overall slightly better. Furthermore, at the nucleate boiling region where the presence of bubbles is intense inclinations of 0° and 30° perform poorer than other inclinations.

Fig. 4 shows that both ONB and OBR vary with θ and G. In general, the effect of G is more profound than the effect of θ. Increasing G, leads ONB (Fig. 4a) and OBR (Fig. 4b) to higher q″ values for all the examined inclinations. This means that boiling phenomena start at higher supplied energy which, in turn, indicates that CHF might be also shifted to higher ΔT_{wall}. This is quite expected because increasing G decreases the thermal boundary layer thickness and, concurrently, the active nucleation site density, whereas it intensifies bubbles' shearing off the wall; all these effects can delay boiling initiation and/or boiling development [27,34].

On the other hand, increasing θ leads to the opposite direction and decreases q″ for both ONB and OBR for all the examined mass fluxes. The decrease is roughly linear, given the experimental uncertainty. Moreover, this linear trend is comparable among the employed mass fluxes. This means that, regardless the G value, as θ increases boiling phenomena start at lower supplied energy, thus the system is efficient already at lower ΔT_{wall}. Unfortunately, CHF might occur also at lower ΔT_{wall}.

There is no easy answer on how inclination may affect the active nucleation site density in boiling. Nevertheless, there is experimental evidence that as θ increases nucleation site density increases, too, and coalescence of neighboring bubbles is promoted [5]. In addition, it is known that heat flux variation with the working conditions in flow boiling (G, θ) is also dictated by the bubbles ability to detach [11]. Examining the role of buoyancy force in this direction, it is seen that at 0° the entire force ($\rho \cdot g \cdot V_b$) is oriented normal to the boiling surface and so it acts as a purely detachment force. At θ: 30-60° only the component normal to the surface, $\rho \cdot g \cdot \cos\theta \cdot V_b$, acts as a detachment force while the component parallel to the surface acts as a sliding force. At 90°, the entire buoyancy force is parallel and concurrent to the flow, so there is no component to contribute to bubble detachment but it all acts as a sliding force. At θ: 120-150° both the normal and parallel buoyancy components make bubbles to accumulate against the heated surface restricting their sliding and detachment, and finally resulting in covering the whole surface with vapor. This is an undesired condition because it blocks heat transfer. In subcooled flow boiling, further to the common body and interfacial forces one should also account for Marangoni stresses created by the steep temperature profile around a bubble and the vapor recoil effect, associated with the bubble thermal sublayer which may disturb significantly the force balance on a bubble [20,22,35]. To this end, it can be argued that the q″ value removed for each θ value results from a combination of effects, namely, the number and proximity of active nucleation sites as well as the bubbles ability to detach.

Fig. 5 offers a global comparison of all boiling curves for the three

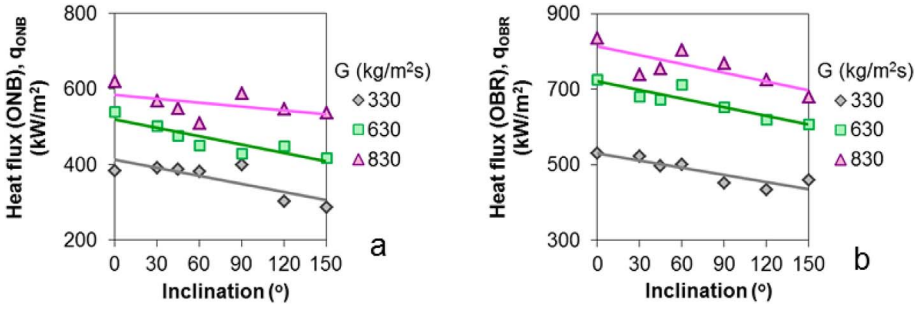

Fig. 4. Effect of mass flux on heat flux (a) of the onset of nucleate boiling (ONB) and (b) of the onset of bubbly regime (OBR).

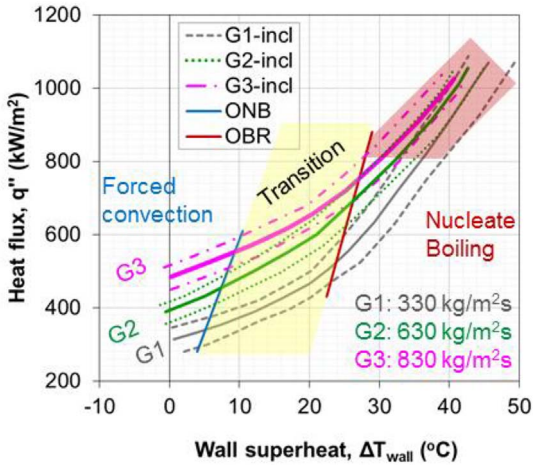

Fig. 5. Effect of mass flux on boiling curves. Solid line: average curve, dashed line: deviation 0-150°.

examined mass fluxes and for all the examined inclinations. Dashed lines indicate the range of deviation of the boiling curves from an average intermediate curve when θ varies within 0-150° (the exact location of the curve for each θ is shown in Fig. 3). It is evident that the effect of mass flux, G, on the boiling curves is higher than the effect of inclination, θ. At the forced convection region, heat removal is influenced heavily by G, as expected, since the dominant heat transfer mechanism in the single-phase liquid flow is forced convection (natural convection can be safely ignored for the examined mass fluxes). At the transition region (yellow area) the presence of bubbles leads to a small widening of the distance between dashed lines (θ-band) which indicates an increasing influence of inclination on heat removal. At the nucleate boiling region, the effect of G diminishes (boiling curves largely converge), while the θ-band gets even wider so the effect of inclination gets also higher. All in all, it could be argued that at high q″ (> 800 kW/m^2, red area), where nucleate boiling dominates, heat transfer cannot be enhanced anymore by increasing G, but this can be achieved to some extent by adjusting θ.

3.1.2. Heat transfer coefficient

In this study water enters the channel at high degree of subcooling (ΔT_{sub} = 70°) and as a result boiling occurs only inside the thermal boundary layer over the heated surface. Fig. 6 presents values of the computed average heat transfer coefficient, h, at different experimental conditions (G, θ, q″). Plots in Fig. 6 are in 2D polar coordinates with h shown in the radial axis and θ in the angular axis while G is a parameter in each plot. For clarity, each of the three displayed plots is for a distinct q″ value (500, 800 and 1000 kW/m^2). Small inset plots at the top right side of polar plots illustrate the ratio of h at different θ vs h at 0°. Overall, the computed h values lie between 5 and 10 kW/m^{2}K, which is a reasonable range for the employed experimental conditions (see discussion in Fig. 7). All experimental values of h, $T_{water,\ out}$, ΔT_{wall} and q″ are included in Tables S1, S2 and S3.

- At 500 kW/m^2 heat transfer occurs in the transition region for G = 330 and 630 kg/m^{2}s and in the forced convection region for G = 830 kg/m^{2}s, (Fig. 5). As expected, h depends on both G and θ, Fig. 6a. For G = 330 and 630 kg/m^{2}s h increases by ~5–10% for all θ values other than 0°. For G = 830 kg/m^{2}s h barely varies with θ (± 2%) due to the absence of bubbles on the heated wall. In all cases, a marginal higher h is computed for 90°.
- At 800 kW/m^2 heat transfer occurs in the low ΔT_{wall} bubbly regime, (Fig. 5). As expected, h shows very small dependence on G; lines in the polar plot are very close to each other, Fig. 6b. For all G values, h exhibits a local maximum at 60°. This maximum enhancement is ~10% for the 330 kg/m^{2}s case but only ~5% for the 630 and 830 kg/m^{2}s cases.
- At 1000 kW/m^2 heat transfer occurs in the high ΔT_{wall} bubbly regime, (Fig. 5), where h is independent of G. A local maximum of h appears at 60° but only ~5% better than at 0°, while for most of the other inclinations h barely varies (max 2%). At this high q″ value, bubbles create intense agitation near the wall which is likely the control mechanism of heat transfer enhancement.

Several empirical relations have been proposed for the determination of h in both single-phase flow and two-phase flow boiling in macrochannels and tubes. In this study, experimental h values are compared to predictions of h from correlations developed by Gnielinski [30] for single-phase flow, and by Liu and Winterton [31] as well as by Shah [32] for two-phase flow boiling (correlations described in section 2.2). The values of the present experimental parameters (G, q″, D_h, α, Re, p_r, Bo, ΔT_{sub}, ΔT_{wall}) fall within the range of applicability of these correlations. Forced convection single-phase heat transfer is not affected by θ so correlation [30] is suitable for all inclinations. Two-phase flow boiling heat transfer is affected by θ, but correlations [31] and [32] are valid both for horizontal and vertical orientation. Results for all θ (0-150°) are illustrated in Fig. 7. Experimental h values for single-phase flow lie between −10 and −40% of the values predicted by Gnielinski [30] (model's tolerance ± 15%) with a MAPE of 23.1% (Fig. 7a). Experimental h values for two-phase flow boiling lie between −20 and −40% of the values predicted by Liu and Winterton (model's tolerance ± 40%) with a MAPE of 31.9% (Fig. 7b), and between ± 35% of the values predicted by Shah (model's tolerance ± 30%) with a MAPE of 21.1% (Fig. 7c). Experimental data show fair agreement with all

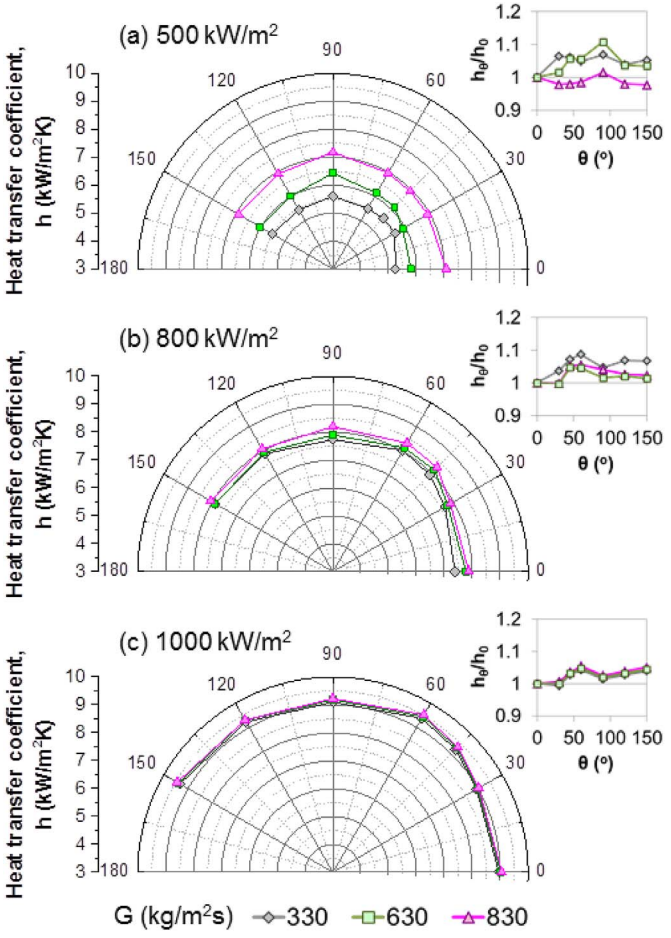

Fig. 6. Effect of channel inclination angle on heat transfer coefficient for different mass and heat fluxes (a) 500 kW/m^2, (b) 800 kW/m^2 and (c) 1000 kW/m^2.

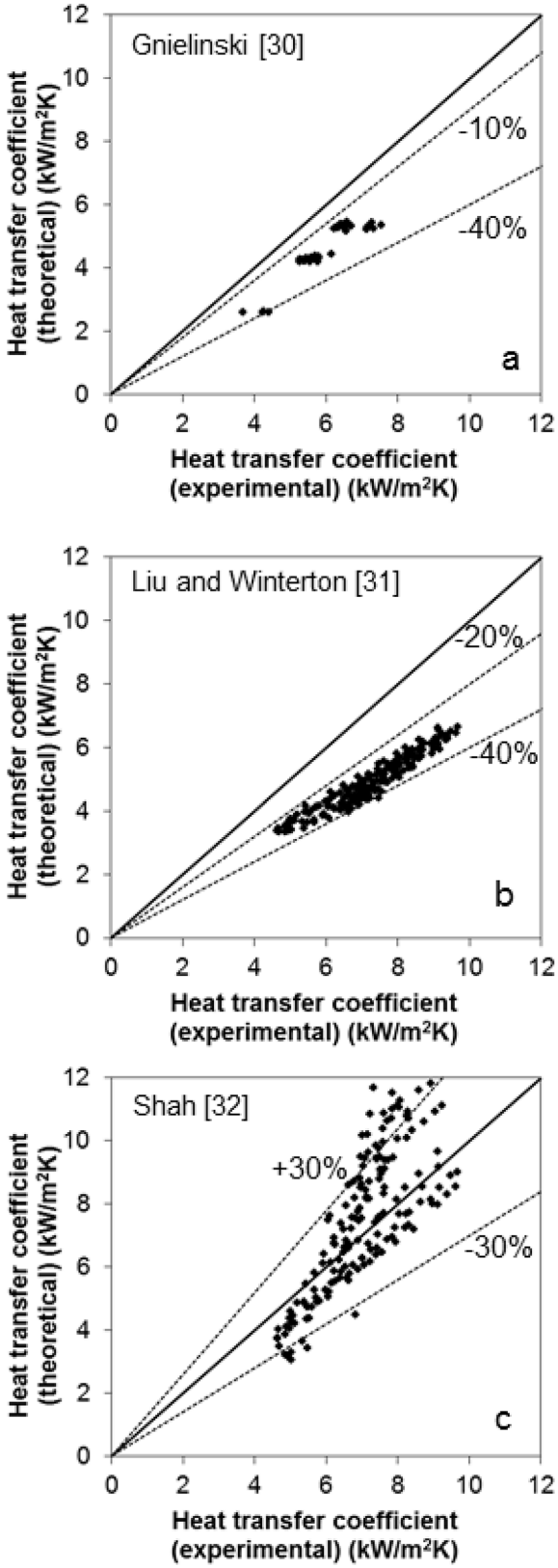

Fig. 7. Comparison between the calculated heat transfer coefficients using correlations and the current experimental values for all inclinations (a) with Gnielinski [30] for single phase, and with (b) Liu and Winterton [31] and (c) Shah [32] for two-phase.

three correlations apart from a few outliers lying outside the tolerance of Shah's model. Those values correspond to the highest employed q″ values for θ: 30-150°. Although steadily deviating by about −30%, the predictions of Liu and Winterton seem to group better the general trend of the current data.

Using T_f instead of the suggested T_{ave} in determining material properties in the aforementioned models has only a marginal impact on the predicted values. On the contrary, the comparison with Liu and Winteton predictions improves appreciably and falls within a ~-20% tolerance limit (MAPE 19.7%) if the exponent of Re in eq. (14) is zeroed while still capturing adequately the general data trend. But it is unrealistic to cancel the varying flow (Re) effect in the model. Regarding the forced convection single phase model of Dittus and Boelter (eq. (17)), using the heated equivalent diameter D_{HP} instead of the hydraulic D_h as the characteristic length in Re and in Nu, leads most of the data points to be in range of ± 30% and MAPE decreases to 19.8% (supplementary S4). Gnielinski's model describes better single phase heat transfer results than Dittus-Boelter model. When Gnielinski's model is incorporated in Shah's equations, it makes the comparison with experimental flow boiling h values better for G = 330 kg/m^{2}s but worse for 630 and 880 kg/m^{2}s (MAPE for all G 27.6%). Apart from it, the spread of the present data is more consistent with Shah's limits of tolerance if the exponent of Boiling number, Bo (eq. (16)), changes to 0.53 (MAPE 19.9%). Yet, the data are still scattered without a clear general trend.

3.2. Effect of inclination on bubble dynamics

3.2.1. Bubbles' behavior

Within the employed field of view one can roughly distinguish different types of moving bubbles: (a) bubbles sliding along the surface at approximately constant size with no detachment, (b) bubbles initially sliding then detaching and then drifting about the surface at approximately constant size, (c) bubbles initially sliding then detaching and then vanishing (fully re-condensing), (d) bubbles lifting-off their nucleation site and then drifting about the surface at approximately constant size and, finally, (e) bubbles lifting-off their nucleation site and then vanishing (fully re-condensing). Cases (a) and (e) are the most common, Fig. 8.

The majority of bubbles, (case a), are sliding along the heated wall without changing dramatically in size, (Fig. 8a). Bubbles size stays approximately the same because at their base bubbles absorb heat from the wall and grow as they slide whereas at their apex they partly re-condense into the colder liquid layers.

In addition, there are several bubbles, (case e) that emerge and vanish in less than a millisecond, without any sign of sliding, Fig. 8b, supplementary material S5. These bubbles are encountered at high heat fluxes and are larger than bubbles of case (a). They are attached onto the surface, grow rapidly and collapse during their detachment because of the high degree of subcooling. These bubbles are considered as the detaching ones in the present work. A plausible explanation of their behavior is as follows. Driven by the high heat flux these bubbles grow excessively fast and almost instantly reach a size much larger than the size of sliding bubbles. When this happens, an appreciable part of these bubbles is exposed to the much colder liquid layers away from the hot wall, above the superheated micro-layer (> 100 °C). Right away these bubbles start re-condensing and as they abruptly shrink they create a wake which brings cold bulk liquid to the wall that is capable of condensing them fully [36,37]. The different size between sliding and re-condensing bubbles is evident in Fig. 8.

As discussed with regard to Fig. 4, bubble detachment or lift-off depends on a number of forces acting on a bubble including disturbances brought about by Marangoni stresses and vapor recoil at the hot surface. According to Situ et al. [20], bubble detachment is controlled by liquid inertia and wall superheat, represented by the Reynolds number and the Jacobs number, respectively. For the specific case of 90°, Fig. 9 displays experimental data in comparison with pertinent literature [1,20,38]. Ahmadi et al. [35], who conducted flow boiling experiments with water at vertical upwards orientation and Re:

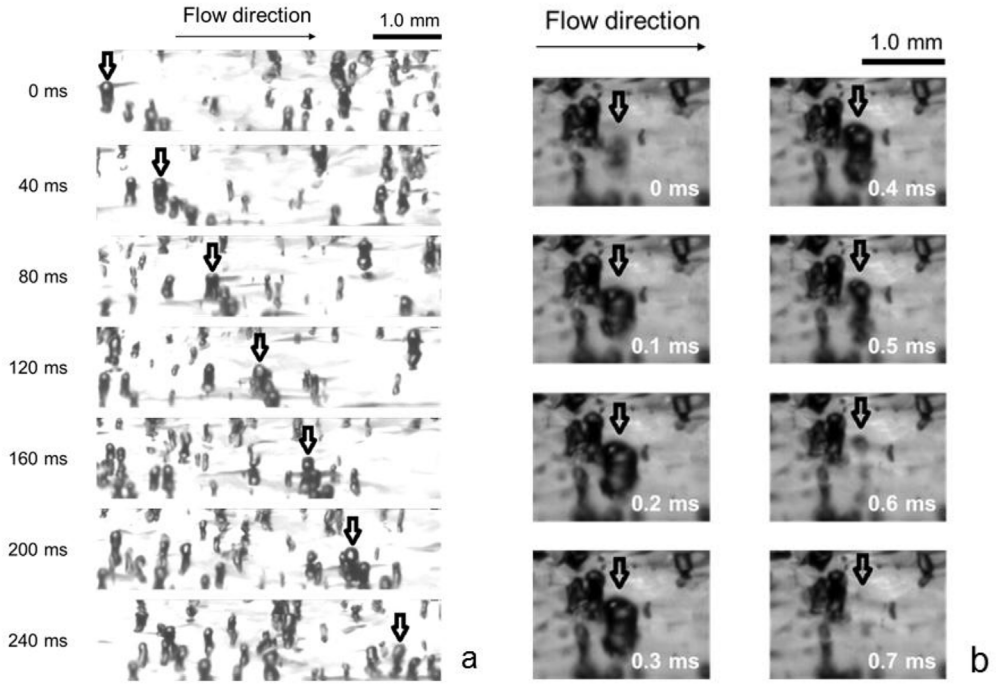

Fig. 8. Images of (a) sliding bubble (8000 fps) at 60°, 630 kg/m^{2}s, 450 kW/m^2 (b) lift-off/re-condense bubble (10000 fps) at 0°, 330 kg/m^{2}s, 600 kW/m^2.

6800–47500 argued that if Ja < 15 bubbles slide, if Ja > 35 they detach and if Ja is in-between, both bubbles behaviors occur. The experimental data of Thorncorft et al. [1], Situ et al. [20] and Basu et al. [38] agree with this criterion. In the present experiments although it is 14 < Ja < 100, the vast majority of bubbles were sliding instead of detaching in all working conditions whereas, based on this criterion, the opposite would be expected. This could be attributed to the presence of dissolved air, which has been argued [22] that in the case of subcooled flow boiling of water favors the presence of sliding bubbles. This is indeed our case as it was not easy to promptly degas 500 L of water before the experiments. In addition, the high degree of subcooling causes vapor bubbles to rapidly re-condense and collapse after their lift off. As heat flux increases, the detaching bubbles become more, due to the increase in the heated wall temperature, which is the driving force of detachment [35].

Fig. 10 illustrates representative snapshots from high speed video recordings for a specific heat flux, 550 ± 50 kW/m^2, for all examined inclinations and all examined mass fluxes. It is apparent that both θ and G affect bubbles features. Image analysis of these high speed video recordings provides detailed information about bubbles size, density and velocity (see next). It must be stressed that the analysis refers strictly to sliding non-detaching bubbles as these represent the vast majority of bubble population.

3.2.2. *Bubbles' size and density*

Bubble size distributions for q″ = 550 ± 50 kW/m^2 and for q″ = 800 ± 10 kW/m^2, having as parameters G and θ values, are presented in Figs. 11 and 12, respectively. All distributions are right-skewed. At low q″ bubble size distributions are narrower (smaller bubbles) and reach higher frequencies than at high q″ (for the same G and θ). In order to get a clearer picture about the effect of the different parameters (q″, G, θ) on bubble size distributions, the quantities of mean, median, mode and standard deviation for 550 ± 50 and 800 ± 10 kW/m^2 are presented in Tables S6 and S7.

Fig. 13 shows the effect of G and θ on the mean diameter of sliding bubbles for 550 ± 50 and 800 ± 10 kW/m^2. Error bars stand for the standard deviation of bubbles populations. Despite the large error bars, there is a fair trend of decreasing d with increasing G at most inclinations. This is consistent with literature [1,19] but it is also realistic on physical grounds because higher G values increase the shearing action of liquid flow and so enhance bubble detachment at smaller diameters. This trend is not easily discernible in the present case because all the

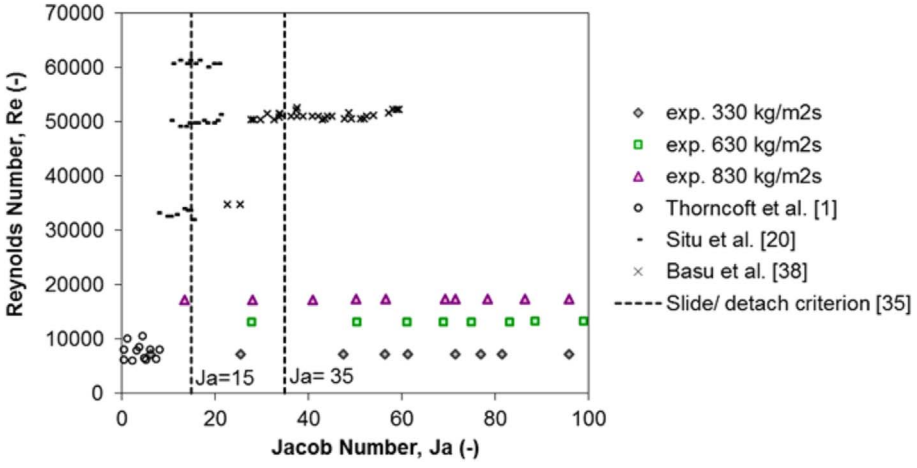

Fig. 9. Comparison of experimental data with literature at vertical upwards orientation (90°).

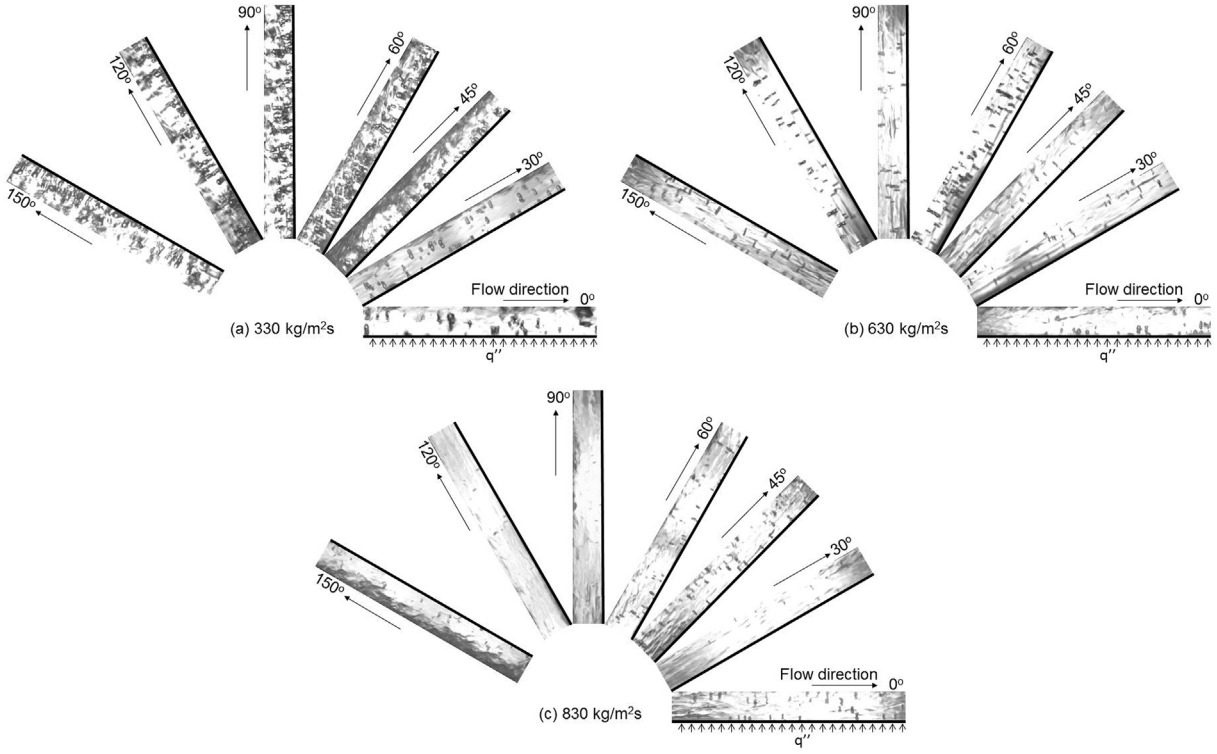

Fig. 10. Images of bubbles for 550 ± 50 kW/m^2, for different inclinations and mass fluxes (a) 330 kg/m^{2}s, (b) 630 kg/m^{2}s and (c) 830 kg/m^{2}s.

examined G values are already high enough. The comparison between Fig. 13a and b shows that d increases as q″ increases as a result of the increased bubble growth rate [1,19]. At higher q″, the standard deviation also increases, an observation reported also by Klausner et al. [39] who associated this with the spatial and temporal fluctuations of the wall superheat which affect the bubble growth rate. Concerning the effect of θ on d, the large errors bars indicate comparable diameters among inclinations. However, one might still be tempted to argue that

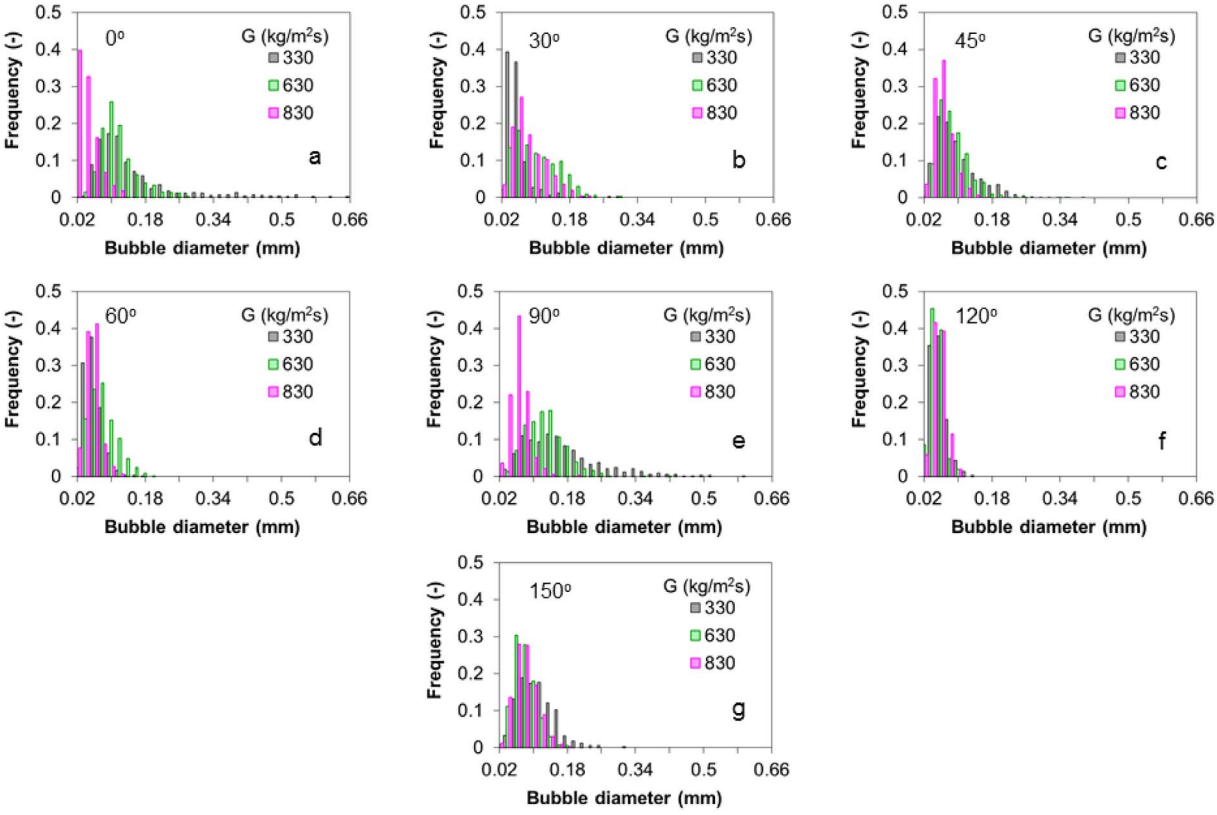

Fig. 11. Bubble size distributions for heat flux 550 ± 50 kW/m^2 and different mass fluxes and inclinations (a) 0°, (b) 30°, (c) 45°, (d) 60°, (e) 90°, (f) 120° and (g) 150°.

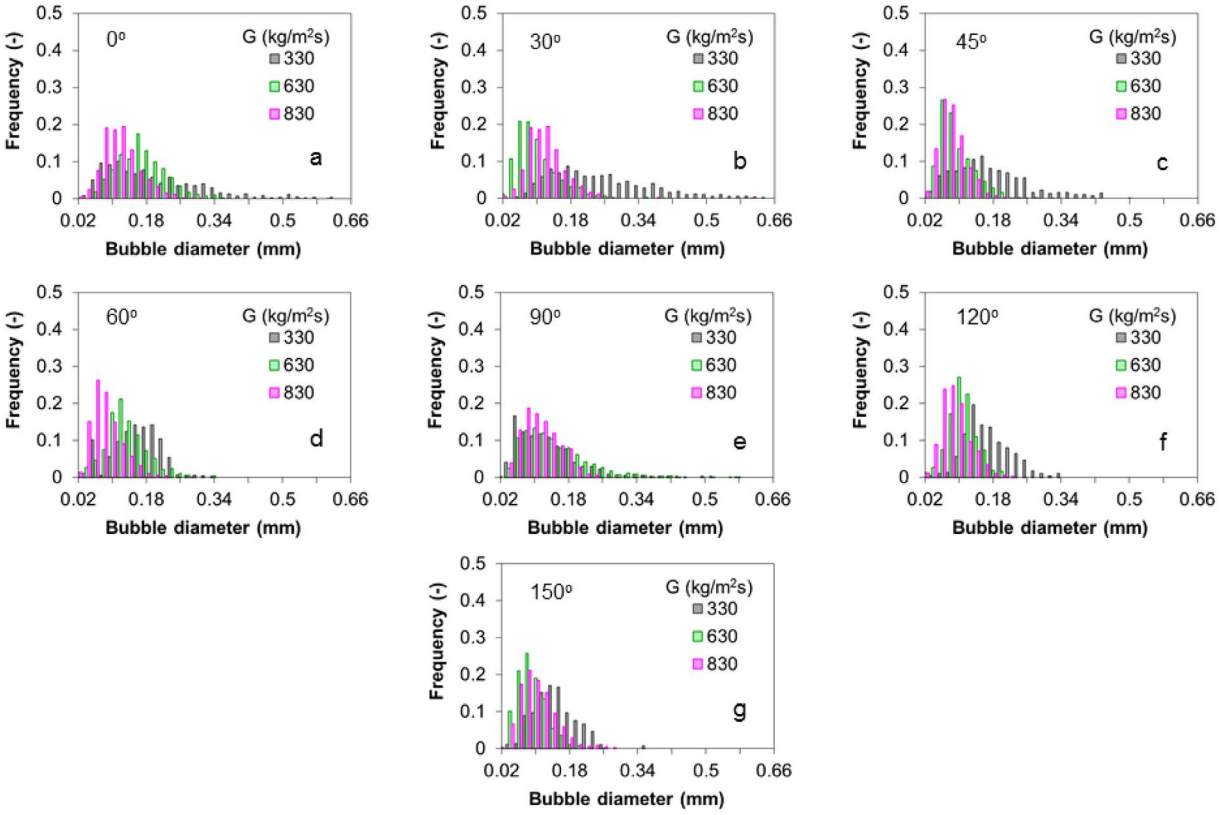

Fig. 12. Bubble size distributions for heat flux 800 ± 10 kW/m^2 and different mass fluxes and inclinations (a) 0°, (b) 30°, (c) 45°, (d) 60°, (e) 90°, (f) 120° and (g) 150°.

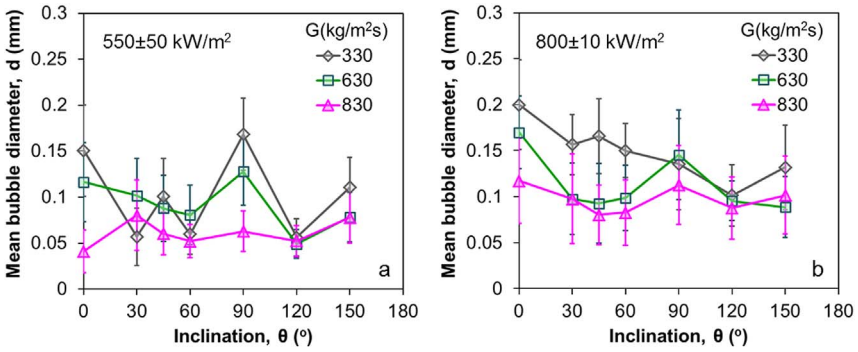

Fig. 13. Effect of channel inclination angle on mean sliding bubble diameter for different mass and heat fluxes (a) 550 ± 50 kW/m^2 and (b) 800 ± 10 kW/m^2.

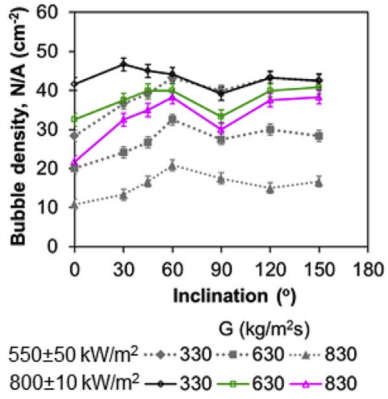

Fig. 14. Effect of channel inclination angle on bubble density for 550 ± 50 and 800 ± 10 kW/m^2.

as G decreases (and inertial forces weaken) the effect of θ is intensified showing subtle local peaks at θ = 0° and 90°. It must be noted that the size of sliding vapor bubbles, as long as detachment does not occur, is associated chiefly with thermal driving forces (heat flux, wall superheat) which dictate their growth. At different inclinations one might expect the varying buoyancy to affect bubble shape and motion as well as natural convection to affect heat transfer to the flowing liquid. However, the contribution of buoyancy and natural convection is insignificant at the high mass flow rates of the present experiments. Moreover, Fig. 6 (inset plots) shows that values of heat transfer coefficient vary by less than ~10% among inclinations so one should not expect thermal forces to affect so much bubble growth as inclination varies [40]. Combining the above, it is not surprising that the mean sliding bubble diameter is pretty constant in all inclinations.

Apart from bubbles size, bubbles density also varies with q″, G and θ. This can be seen in Fig. 14, where the number of bubbles over surface

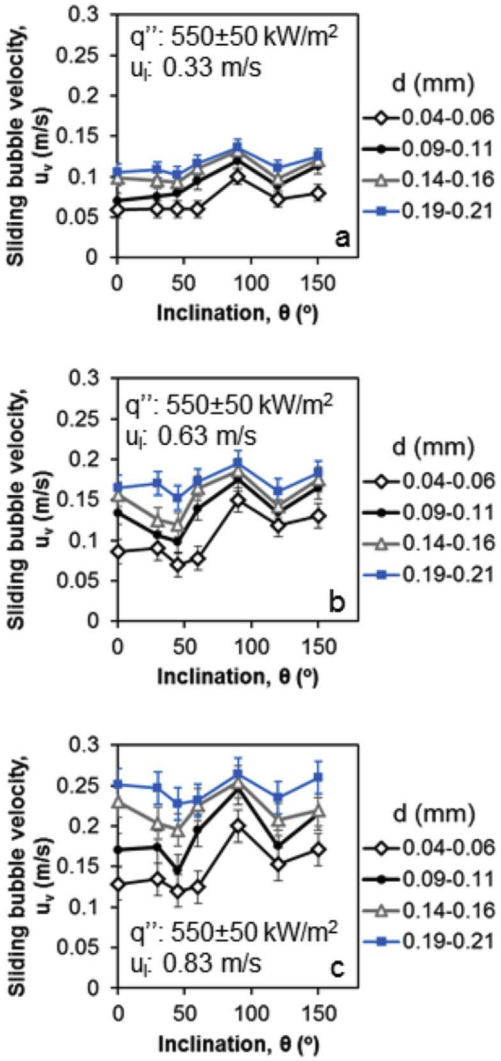

Fig. 15. Effect of channel inclination angle on mean sliding bubble velocity for 550 ± 50 kW/m^2 and (a) 330 kg/m^{2}s, (b) 630 kg/m^{2}s, (c) 830 kg/m^{2}s.

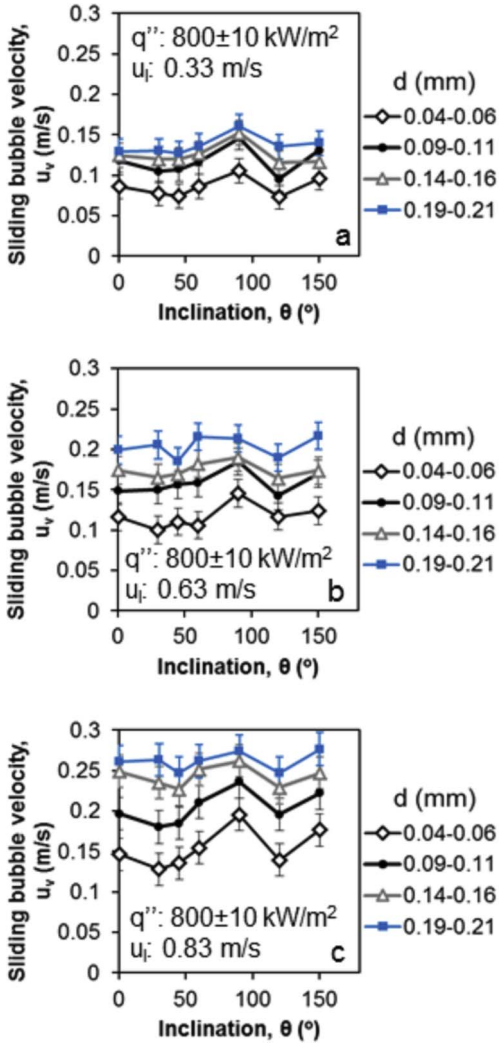

Fig. 16. Effect of channel inclination angle on mean sliding bubble velocity for 800 ± 10 kW/m^2 and (a) 330 kg/m^{2}s, (b) 630 kg/m^{2}s, (c) 830 kg/m^{2}s.

area, N/A, is plotted against θ for the same q″ and G, as in Fig. 13. As with the bubble size, higher q″ and lower G yield higher N/A, due to the larger number of active nucleation sites. Furthermore, N/A increases with θ until a local maximum at 30-60°, and thereafter it either slightly decreases or stays almost constant. These trends agree with qualitative observations in Fig. 10 and reflect small variations of the wall superheat with inclination (boiling curves, Fig. 3) which affect directly the number of active nucleation sites. This observation agrees with literature and recent pool boiling experiments performed by Jung and Kim [5].

3.2.3. Bubbles' sliding velocity

Fig. 15 presents bubbles sliding velocity, u_v, for four distinct mean diameter, d, values, namely, 0.05, 0.10, 0.15 and 0.20 mm (± 0.01 mm) at 550 ± 50 kW/m^2. Results for all three mass fluxes, G, are displayed. The respective mean liquid velocities, u_l, over the cross-section of the channel are 0.33, 0.63 and 0.83 m/s. It is noticed that u_v is lower than u_l by about 70% in all cases which reflects chiefly the reduced liquid velocity near the wall. It is also noticed that u_v increases with d but not in a proportional manner probably reflecting the non-linear velocity profile near the wall.

As q″ rises at 800 ± 10 kW/m^2, Fig. 16, bubbles appear to slide a bit faster. This has been attributed to higher bubble growth rates [23] but it may be also a result of the lower viscosity of the hotter liquid layers near the wall. As regards the effect of θ on u_v, it seems that a maximum is observed at 90° especially for smaller bubbles (d < 0.10 mm). This is not surprising, as at 90° buoyancy acts parallel to the main flow direction, contributing to u_v [23]. It must be noted that the contribution of buoyancy at the different inclinations in the velocity of sliding bubbles is small. For instance, for bubbles with d = 0.1 mm the observed sliding velocity is 20–50 times larger than the buoyancy velocity calculated by Stokes' law, for the horizontal channel, and even larger for the inclined cases ($u_{byoyancy}$ is proportional to cosθ).

Bubble dynamics presented in section 3.2 are consistent with the thermal characteristics identified in section 3.1. As mass flux increases both the size and density of bubbles decrease (Figs. 13 and 14) because of the decrease in the heated wall temperature and the forced convection domination, whereas their velocity increases (Fig. 15). Thus, when G increases, the contribution of forced convection is more prominent than nucleate boiling and the transition region extends to higher wall superheats and higher heat fluxes as shown in Fig. 5. As channel inclination increases, bubble size and bubble velocity show a modest peak at θ = 90° whereas bubbles density exhibits a reasonable peak between 30° and 60°. These features are in line with the observed local maxima of heat transfer coefficient, h, between 60° and 90° as presented in Fig. 6.

4. Conclusions

This study explores the influence of inclination between 0° and 150° on subcooled flow boiling heat transfer in a macrochannel (10 × 40 × 120 mm) under atmospheric pressure. Water is used as working fluid at 30 °C inlet temperature, at three mass velocities, 330, 630 and 830 kg/m^{2}s and at heat flux conditions between 300 and 1000 kW/m^2. Temperature recordings and high-speed video imaging are used to characterize thermal performance and identify bubbles dynamics.

Boiling curves present three dominant heat transfer regions: forced convection, transition and nucleate boiling. Onset of nucleate boiling (ONB) and onset of bubbly regime (OBR) vary with inclination and mass flux. Mass flux has a stronger effect than inclination on boiling curves but, even so, inclinations of 60° and 90° lead to slightly higher heat fluxes. The experimentally determined heat transfer coefficient values lie between 5 and 10 kW/m^{2}K and agree reasonably with predictions of well-known empirical correlations from literature.

The role of inclination on heat removal rates is discussed with respect to the density of active nucleation sites and bubbles type of motion on the boiling surface. Furthermore, analysis of high speed video recordings illustrate that bubbles mean diameter is comparable among inclinations with a bit higher value at 90° where bubbles sliding velocity also shows a mild maximum. On the other hand, bubbles density exhibits a local maximum at 30–60°. These features are consistent with the observed maximum of heat transfer coefficient between 60° and 90°.

Acknowledgements

This research was supported by the European Space Agency (Contract No. 4000106405/12/NL/PA on highly efficient flow boiling macrostructured/macroporous channels) and IKY Fellowships of Excellence for Postgraduate Studies in Greece (the SIEMENS Program). The work was performed under the umbrella of COST Action MP1106.

Appendix A. Supplementary data

Supplementary data related to this article can be found at http://dx.doi.org/10.1016/j.ijthermalsci.2017.10.041.

References

[1] G.E. Thorncroft, J.F. Klausner, R. Mei, An experimental investigation of bubble growth and detachment in vertical upflow and downflow boiling, Int J Heat Mass Transf 41 (1998) 3857–3871.
[2] W.M. Rohsenow, J.P. Hartnett, Y.I. Cho, Handbook of heat tranasfer, McGraw-Hill, USA, 1998.
[3] C.W.M. Van Der Geld, C. Colin, Q.I.E. Segers, V.H. Pereira da Rosa, H.N. Yoshikawa, Forces on a boiling bubble in a developing boundary layer, in microgravity with g-jitter and in terrestrial conditions, Phys Fluids 24 (2012) 082104.
[4] M.S. El-Genk, A. Suszko, Effects of inclination angle and liquid subcooling on nucleate boiling on dimpled copper surfaces, Int J Heat Mass Transf 95 (2016) 650–661.
[5] S. Jung, H. Kim, Effects of surface orientation on nucleate boiling heat transfer in a pool of water under atmospheric pressure, Nucl Eng Des 305 (2016) 347–358.
[6] S. Jun, J. Kim, S.M. You, H.Y. Kim, Effect of heater orientation on pool boiling heat transfer from sintered copper microporous coating in saturated water, Int J Heat Mass Transf 103 (2016) 277–284.
[7] C.W.M. Van Der Geld, C.H.M. Baltis, G.J.M. Priems, Forces on rapidly growing vapor bubbles on a wall in forced convection with varying angle of inclination, Colloid Surf A 505 (2016) 29–36.
[8] S.G. Kandlikar, W.J. Grande, Evolution of microchannel flow passages-thermohydraulic performance and fabrication technology, Heat Transf Eng 24 (2003) 3–17.
[9] T. Harirchian, S.V. Garimella, Boiling heat transfer and flow regimes in microchannels - a comprehensive understanding, ASME J Electron Pack 133 (2011) 011001.
[10] V.K. Dhir, H.S. Abarajith, D. Li, Bubble dynamics and heat transfer during pool and flow boiling, Heat Transf Eng 28 (2007) 608–624.
[11] H. Zhang, I. Mudawar, M.M. Hasan, Experimental assessment of the effects of body force, surface tension force, and inertia on flow boiling CHF, Int J Heat Mass Transf 45 (2002) 4079–4095.
[12] R. Situ, T. Hibiki, M. Ishii, M. Mori, Bubble lift-off size in forced convective subcooled boiling flow, Int J Heat Mass Transf 48 (2005) 5536–5548.
[13] C.R. Kharangate, L.E. O'Neill, I. Mudawar, Effects of two-phase inlet quality, mass velocity, flow orientation, and heating perimeter on flow boiling in a rectangular channel: Part 1–two-phase flow and heat transfer results, Int J Heat Mass Transf 103 (2016) 1261–1279.
[14] M.A. Akhavan-Behabadi, M. Esmailpour, Experimental study of evaporation heat transfer of R-134a inside a corrugated tube with different tube inclinations, Int Commun Heat Mass Transf 55 (2014) 8–14.
[15] A. Kundu, R. Kumar, A. Gupta, Flow boiling heat transfer characteristics of R407C inside a smooth tube with different tube inclinations, Int J Refrig 45 (2014) 1–12.
[16] H. Zhang, I. Mudawar, M.M. Hasan, Experimental and theoretical study of orientation effects on flow boiling CHF, Int J Heat Mass Transf 45 (2002) 4463–4477.
[17] C. Konishi, I. Mudawar, M.M. Hasan, Investigation of the influence of orientation on critical heat flux for flow boiling with two-phase inlet, Int J Heat Mass Transf 61 (2013) 176–190.
[18] C.R. Kharangate, L.E. O'Neill, I. Mudawar, M.M. Hasan, H.K. Nahra, R. Balasubramaniam, et al., Effects of subcooling and two-phase inlet on flow boiling heat transfer and critical heat flux in a horizontal channel with one-sided and double-sided heating, Int J Heat Mass Transf 91 (2015) 1187–1205.
[19] R. Sugrue, J. Buongiorno, T. McKrell, An experimental study of bubble departure diameter in subcooled flow boiling including the effects of orientation angle, subcooling, mass flux, heat flux, and pressure, Nucl Eng Des 279 (2014) 182–188.
[20] R. Situ, M. Ishii, T. Hibiki, J.Y. Tu, G.H. Yeoh, M. Mori, Bubble departure frequency in forced convective subcooled boiling flow, Int J Heat Mass Transf 51 (2008) 6268–6282.
[21] Y.A. Zeigarnik, D.N. Platonov, K.A. Khodakov, Y.L. Shekhter, Visualization of boiling of subcooled water, High Temp 49 (2011) 566–570.
[22] Y.A. Zeigarnik, K.A. Khodakov, Y.L. Shekhter, Experimental data on the mechanism of subcooled water boilng: high-speed video shootings, Thermophys Aeromech 21 (2014) 285–292.
[23] D.-w. Yuan, L.-m. Pan, D. Chen, H. Zhang, J.-h. Wei, Y.-p. Huang, Bubble behavior of high subcooling flow boiling at different system pressure in vertical narrow channel, Appl Therm Eng 31 (2011) 3512–3520.
[24] P. Guan, L. Jia, L. Yin, Z. Tan, Bubble departure size in flow boiling, Heat Mass Transf 51 (2014) 921–930.
[25] R. Ahmadi, T. Okawa, Influence of surface wettability on bubble behavior and void evolution in subcooled flow boiling, Int J Therm Sci 97 (2015) 114–125.
[26] C.L. Vandervort, A.E. Bergles, M.K. Jensen, An experimental study of critical heat flux in very high heat flux subcooled boiling, Int J Heat Mass Transf 37 (1994) 161–173.
[27] M.C. Vlachou, J.S. Lioumbas, K. David, D. Chasapis, T.D. Karapantsios, Effect of channel height and mass flux on highly subcooled horizontal flow boiling, Exp Therm Fluid Sci 83 (2017) 157–168.
[28] T.D. Karapantsios, S.P. Evgenidis, K. Zacharias, T. Mesimeris, European Patent Office (Ed.), Method for the detection and characterization of bubbles in liquids and device therefor, resp. system, 2015.
[29] B. Tóth, Development, E. s. S. M. P. Operations teams, S. Teams and S. Industry, Future experiments to measure liquid-gas phase change and heat transfer phenomena on the International Space Station, Microgravity Sci Tec 24 (2011) 189–194.
[30] V. Gnielinski, New equations for heat and mass transfer in turbulent pipe and channel flow, Int Chem Eng 16 (1976) 359–368.
[31] Z. Liu, E.H.S. Winterton, A general correlation for saturated and subcooled flow boiling in tubes and annuli, based on a nucleate pool boiling equation, Int J Heat Mass Transf 32 (1991) 2759–2766.
[32] M.M. Shah, New correlation for heat transfer during subcooled boiling in plain channels and annuli, Int J Therm Sci 112 (2017) 358–370.
[33] F.W. Dittus, L.M.K. Boelter, Heat transfer in automobile radiators of the tubular type, University of California Press, California, 1930.
[34] H. Steiner, A. Kobor, L. Gebhard, A wall heat transfer model for subcooled boiling flow, Int J Heat Mass Transf 48 (2005) 4161–4173.
[35] R. Ahmadi, T. Ueno, T. Okawa, Bubble dynamics at boiling incipience in subcooled upward flow boiling, Int J Heat Mass Transf 55 (2012) 488–497.
[36] H. Kalman, Y.H. Mori, Experimental analysis of a single vapor bubble condensing in subcooled liquid, Chem Eng J 84 (2002) 197–206.
[37] T. Yabuki, O. Nakabeppu, Microscale wall heat transfer and bubble growth in single bubble subcooled boiling of water, Int J Heat Mass Transf 100 (2016) 851–860.
[38] N. Basu, G.R. Warrier, V.K. Dhir, Wall heat flux partitioning during subcooled flow boiling: Part 1-Model development, J Heat Transf 127 (2005) 131.
[39] J. Klausner, R. Mei, D. Bernhard, L. Zeng, Vapor bubble departure in forced convection boiling, Int J Heat Mass Transf 36 (1993) 651–662.
[40] Y.-N. Kim, J.S. Kim, G.C. Park, H.K. Cho, Measurement of sliding bubble behavior on a horizontal heated tube using a stereoscopic image processing technique, Int J Multiph Flow 94 (2017) 156–172.